Mismatch in Mechanical and Adhesive Properties Induces Pulsating Cancer Cell Migration in Epithelial Monolayer

Meng-Horng Lee,[†‡] Pei-Hsun Wu,[†‡] Jack Rory Staunton,[§¶] Robert Ros,[§¶] Gregory D. Longmore,[‡§‖**††*] and Denis Wirtz[†‡*]

[†]Department of Chemical and Biomolecular Engineering and [‡]Johns Hopkins Physical Sciences-Oncology Center, The Johns Hopkins University, Baltimore, Maryland; [§]Department of Physics and [¶]Arizona State University Physical Sciences-Oncology Center, Arizona State University, Tempe, Arizona; and [‖]Department of Medicine, **Department of Cell Biology and Physiology, and [††]BRIGHT Institute, Washington University School of Medicine, St. Louis, Missouri

ABSTRACT The mechanical and adhesive properties of cancer cells significantly change during tumor progression. Here we assess the functional consequences of mismatched stiffness and adhesive properties between neighboring normal cells on cancer cell migration in an epithelial-like cell monolayer. Using an in vitro coculture system and live-cell imaging, we find that the speed of single, mechanically soft breast carcinoma cells is dramatically enhanced by surrounding stiff nontransformed cells compared with single cells or a monolayer of carcinoma cells. Soft tumor cells undergo a mode of pulsating migration that is distinct from conventional mesenchymal and amoeboid migration, whereby long-lived episodes of slow, random migration are interlaced with short-lived episodes of extremely fast, directed migration, whereas the surrounding stiff cells show little net migration. This bursty migration is induced by the intermittent, myosin II-mediated deformation of the soft nucleus of the cancer cell, which is induced by the transient crowding of the stiff nuclei of the surrounding nontransformed cells, whose movements depend directly on the cadherin-mediated mismatched adhesion between normal and cancer cells as well as α-catenin-based intercellular adhesion of the normal cells. These results suggest that a mechanical and adhesive mismatch between transformed and nontransformed cells in a cell monolayer can trigger enhanced pulsating migration. These results shed light on the role of stiff epithelial cells that neighbor individual cancer cells in early steps of cancer dissemination.

INTRODUCTION

The mechanical properties of cells can significantly change in the context of disease. For instance, mutations in genes coding for intermediate filament keratins have long been known to induce mechanical softening of the cellular cytoplasm in a wide range of epithelial diseases (1,2). The cytoskeleton of cells from patients and mouse models of muscular dystrophy and progeria are also consistently softer than the cytoskeleton of their wild-type counterparts (3,4). In particular, some of the most significant and reliable functional differences between normal and cancer cells are those observed in their mechanical properties (5). A wide range of approaches, including atomic force microscopy (AFM), cell stretching, and microrheology, have consistently shown that both the cytoplasm and nucleus of cancer metastatic cells are significantly softer than those of nontransformed or nonmetastatic cells (6–10).

During early carcinoma tumor growth in an epithelial sheet, cells of different mechanical stiffnesses are in close contact with one another. The functional consequences of a mechanical mismatch between neighboring normal and cancer cells remains unclear. Specifically, we sought to determine whether differences in mechanical properties could lead to a novel mechanism of cell migration for individual cells in physical contact with one another in a cell monolayer. We devised a coculture system composed of a single layer of nontransformed human epithelial cells, whose cytoplasm and nucleus display a relatively high elastic modulus, and that contain a very low density of individual interdispersed human breast carcinoma cells, whose cytoplasm and nucleus display a relatively low elastic modulus. This model system allowed us to determine whether (and how) the migration of these cancer cells was affected by their physical interactions with the surrounding normal cells of the epithelium.

Our results indicate that the motility of individual breast cancer MDA-MB-231 cells, which are mechanically soft, is dramatically enhanced when they are surrounded by nontransformed breast epithelium MCF10A cells, which are mechanically stiff, compared with single-cell motility within a cluster of MDA-MB-231 cells (high density) or single MDA-MB-231 cells (low density) in the absence of MCF10A cells. We observe that individual MDA-MB-231 cells undergo highly transient bursts of extremely fast migration, which is induced by the temporary crowding of surrounding MCF10A cells. This result is not obvious a priori, because intuition would predict a reduction in motility caused by steric forces mediated by strong cell-cell interactions. This bursty migration is caused by the differential stiffness of the cytoplasm and nucleus between cancer and normal cells, which in a coordinated manner induces a large, unstable deformation of the nucleus of the cancer cell, which in turn induces its interstitial migration between normal cells. This bursty migration critically depends on

Submitted March 25, 2012, and accepted for publication May 7, 2012.

*Correspondence: wirtz@jhu.edu or glongmor@dom.wustl.edu

Editor: Petra Schwille.

0006-3495/12/06/2731/11 $2.00

doi: 10.1016/j.bpj.2012.05.005

E-cadherin/α-catenin-mediated cell-cell adhesion between normal cells to allow for coordinated squeezing of the cancer cell and a mismatch in cadherin-based adhesion between normal and cancer cells. We also find that the modulation of this bursty migration does not directly depend on soluble factors secreted by nontransformed cells. Hence, these results suggest that differential physical properties can drive the net migration of individual cells with a soft cytoplasm and nucleus, in a dense monolayer of cells of mismatched adhesive and stiffness properties. These results also suggest that normal cells play a previously unknown but critical role in the enhanced migration of metastatic carcinoma cells, which is mediated by E-cadherin cell-cell adhesion of the normal epithelial tissue.

MATERIALS AND METHODS

Cell culture and coculture

Nontransformed human breast epithelial cells (MCF10A), transformed metastatic human breast carcinoma cells (MDA-MB-231), and transformed nonmetastatic human breast carcinoma cells (MCF7) were obtained from the American Type Culture Collection (ATCC, Manassas, VA). MCF10A cells were cultured and passed in 5% horse serum supplemented with 20 ng/ml hEGF, 10 μg/ml insulin, 100 ng/ml cholera toxin, and 0.5 μg/ml hydrocortisone. MDA-MB-231 cells were maintained in Dulbecco's modified Eagle's medium (DMEM) supplemented with 10% fetal bovine serum. MCF7 cells were maintained in DMEM supplemented with 10% fetal bovine serum and 10 μg/ml insulin.

In the coculture experiment, 1×10^4 MDA-MB-231 cells were coseeded with 5×10^5 MCF10A cells in a four-well chamber slide (area per well: 1.8 cm^2; Lab-Tek, Hatfield, PA) with MCF10A medium, and the next day the cells were monitored under fluorescence microscopy for 16 h. For single-cell and confluent conditions, MDA-MB-231 cells were seeded with MCF10A medium to maintain consistent conditions in coculture experiments.

For the conditioned medium collection, 2×10^6 cells were seeded in a one-well chamber slide (Lab-Tek), and 24 h later the conditioned medium were harvested and filtered through a 0.45 μm filter (Millipore, Bedford, MA).

Lentiviral expression constructs

The lentiviral vector of enhanced green fluorescent protein (EGFP; pCS-CG) was purchased from Addgene (Cambridge, MA). The lentiviral vector of lifeact-EGFP and E-cadherin-EGFP were generated from pCS-CG. The sequence of lifeact peptide or full-length E-cadherin was cloned upstream of EGFP between the Nhe1 and Age 1 sites of pCS-CG to generate EGFP-fused protein. The αE-catenin shRNA vector was generated as described before. Briefly, the sequence 5′-GGACCTGCTTTCG GAGTACAT-3′ targeting αE-catenin was cloned downstream of the H1 promoter between the MluI and ClaI sites in pLVTHM lentiviral vector (Addgene).

Lentivirus production and transduction

A second-generation lentivirus was produced as described previously (11). Briefly, 293T cells (ATCC) were transiently cotransfected with three plasmids (lentiviral vector, ΔR 8.91, and pMDG-VSVG) using the standard calcium phosphate precipitation method. After 22–24 h of transfection, the medium was replaced with fresh medium. The lentiviral particles were harvested 24 h later, immediately filtered through 0.45 μm filter (Millipore) to remove cells debris, and then stored at -80°C. For transduction, 1×10^5 cells in a 35-mm culture dish were repeatedly transduced with lentivirus with 8 μg/ml polybrene to reach high transduction (>80%).

Live-cell microscopy

Cells were grown on the coverglass of a four-well chamber slide (Lab-Tek) and the next day the cells were live-stained with Hoechst 33342 (1:2000, room temperature for 5 min; Invitrogen, Eugene, OR). Time-lapse images were collected every 5 min for 16 h using a Nikon TE2000E epifluorescence microscope equipped with a 40× objective (Nikon, Melville, NY) and a Cascade 1K CCD camera (Roper Scientific, Tucson, AZ). A series of time-lapse images were processed and analyzed using NIS-Elements AR software (Nikon) and customized MATLAB (The MathWorks, Natick, MA) analysis software.

AFM measurements of cell mechanics

The mechanical properties of the MDA-MB-231 ($n = 25$) and MCF-10A ($n = 25$) cells were measured by AFM nanoindentation. The cells were seeded on glass-bottomed dishes (Fluorodish; World Precision Instruments, Sarasota, FL) and grown for 24 h before measurements were obtained. Thirty minutes before the measurements were conducted, the cells were stained with nuclear and nucleolar dyes (Nuclear ID Red and Nucleolar ID Green; Enzo Life Sciences, Farmingdale, NY) at 1 μM concentrations and resuspended in 1× imaging assay buffer (Enzo Life Sciences). The cells were imaged with a confocal microscope (Microtime 200; Picoquant, Berlin, Germany) before and after AFM nanoindentation to identify and locate points to indent over the cytoplasmic, nuclear, and nucleolar regions. Each point was indented ~10 times with a loading rate of 2 μm/s and a trigger force of 0.6 nN using a sharp probe (MSNL; Veeco, Santa Barbara, CA) by an MFP-3D BIO AFM (Asylum Research, Santa Barbara, CA) mounted on the optical microscope (IX-71; Olympus, Center Valley, PA). To calculate the depth-dependent Young's moduli from the force-indentation curves, the curves were fitted piecewise as described elsewhere (12). The cells were taken to have a Poisson ratio of 0.5. The AFM probe cantilever spring constants were determined with the use of the AFM software (Asylum Research, Santa Barbara, CA) and the thermal noise method (13).

Cross-correlation analysis

We obtained temporal cross correlations by computing the sequential results of displacement (R) and the aspect ratio of cell shape (ARC) from a 16-h-long movie into the following equation using MATLAB:

$$\rho(\tau) = \frac{\langle (dR(t) - \langle dR(t) \rangle) \times (\mathrm{ARC}(t+\tau) - \langle \mathrm{ARC}(t) \rangle) \rangle}{\sigma_{dR} \times \sigma_{\mathrm{ARC}}},$$

where σ_{dR} and σ_{ARC} represent the standard deviation of data series of $dR(t)$ and $ARC(t)$, respectively.

Immunofluorescence and Western blots

For immunostaining, cells were fixed with 4% paraformaldehyde, permeabilized, and then incubated with the following antibodies: rabbit anti-E-cadherin (1:100, 4°C overnight; Cell Signaling Technology, Danvers, MA), mouse anti-cadherin 11 (1:100, 4°C overnight; Sigma, St. Louis, MO), phalloidin (1:40, room temperature for 20 min; Invitrogen, Eugene, OR) and Hoechst 33342 (1:1000, room temperature for 10 min; Invitrogen). Images of the stained cells were acquired with a Nikon A1 confocal microscope (Nikon) equipped with a 60× plan lens (N.A. 1.2). For Western

blotting, the following antibodies were used: rabbit anti-human αE-catenin (1:1000 in 5% milk; Sigma) and goat anti-actin (1:5000 in 5% milk; Santa Cruz Biotechnology, Santa Cruz, CA) overnight at 4°C.

Statistical analysis

The number of cells examined for each experiment is indicated in the figure captions. The mean ± standard error (SE) was determined and statistical analysis was performed with the use of Graphpad Prism (Graphpad Software, San Diego, CA). Two-tailed unpaired *t*-tests and a one-way analysis of variance were conducted to determine the significance of samples with two groups and more than two groups, as indicated by the standard Michelin Guide scale (***$p < 0.001$, **$p < 0.01$, and *$p < 0.05$).

RESULTS

The migration of single transformed cells is dramatically enhanced in an epithelial-like sheet

To determine whether stiff cells could actively influence the motion of individual soft cells dispersed in an epithelial-like cell monolayer, we chose to use a model system of individual breast carcinoma cells (MDA-MB-231) interdispersed at very low density in a monolayer of nontransformed human breast epithelial cells (MCF10A). First, we determined the mechanical properties of these two cells lines using an atomic force microscope. As expected, these measurements showed that the stiffness of the cytoplasmic region and nucleus of the MDA-MB-231 cells was 1.3- and ~4-fold lower, respectively, than that of the MCF10A cells (Fig. 1 *a*). The migratory behavior of MDA-MB-231 cells was considered in the following three cases: 1), individual (low density) MDA-MB-231 cells; 2), a confluent layer of MDA-MB-231 cells; and 3), single MDA-MB-231 cells scattered in a confluent monolayer of stiff MCF10A cells. In case 3, to distinguish individual MDA-MB-231 cells from surrounding nontransformed cells, MDA-MB-231 cells were stably transfected with EGFP using a lentiviral gene transfer system and mixed at a ratio of 1:50 to MCF10A cells (Fig. 1 *b*).

We evaluated the migratory speed of individual cells by collecting 16-h-long movies of their nucleus, which had been labeled with vital dye Hoechst 33342 (Fig. 1 *b*), and computing the distance traveled by the nucleus centroid between frames recorded every 6 min. We verified that for each cell, the speed of the cell and the speed of its nucleus were statistically similar (see Fig. S1 in the Supporting Material). We also verified that cell speed was unaffected by EGFP transfection and Hoechst 33342 labeling, because the cell speeds of labeled and unlabeled MDA-MB-231 cells were statistically similar (Fig. S2). As expected because, a priori, the surrounding cells would form steric blocks restraining cell motion, the MDA-MB-231 cells in the monolayer (case 2) moved much more slowly than the single MDA-MB-231 cells at low density (case 1). The instantaneous velocity (i.e., the averaged cell displacement divided by time between frames) was significantly reduced and, in particular, the net velocity (i.e., the averaged cell displacement between the first and last positions divided by the total time of movie capture), which measures the ability to undergo net migration as opposed to short-length-scale movements, remained low (Fig. 1, *c–e*). Accordingly, the trajectories of cells in these two cases were both compact (Fig. 1 *c*, Movie S1, and Movie S2).

In striking contrast to the two conventional cases above, single MDA-MB-231 cells in coculture with MCF10A cells (case 3) showed significantly increased instantaneous and net velocities (Fig. 1, *d* and *e*). In particular, the net velocity increased ~2.5-fold compared with single MDA-MB-231 cells without MCF10A cells (Fig. 1 *e* and Fig. S3). The trajectories of carcinoma cells in a monolayer of MCF10A cells showed long, straight, fast portions, reflective of persistent moves interlaced with more random, slow portions when the MDA-MB-231 cells were caged by MCF10A cells (Fig. 1 *c* and 2 *f*, and Movie S3).

The failure of confluent nontransformed cells to constrain the motility of the transformed cells (as in case 2) prompted us to investigate whether the MDA-MB-231 cells were simply detached from the surrounding cells, and whether these cells migrated on top of or, conversely, underneath the monolayer of nontransformed cells. Using time-resolved confocal microscopy, we found that individual MDA-MB-231 cells were fully embedded within the monolayer of MCF10A cells and remained attached to the underlying substratum (Fig. 1 *f*). This implies that the single carcinoma cells had to squeeze between nontransformed cells of the monolayer in order to move, i.e., the MDA-MB-231 cells did not rapidly surf on top of the MCF10A cell monolayer or crawl underneath it.

The dramatically enhanced motility of MDA-MB-231 cells in coculture conditions suggested that these cells might undergo a mode of migration qualitatively different from those of the same cells in the conventional cases (cases 1 and 2). A close examination of the movements of MDA-MB-231 cells in coculture conditions revealed that, from time to time, these cells underwent a dramatic morphological change, transiently switching from a relatively rounded shape to a highly elongated, sometimes dumbbell shape while squeezing between nontransformed cells (Fig. 2 *a*), resulting in large-amplitude bursts of rapid displacements (Fig. 2 *b*). Accordingly, the temporal profile of the instantaneous velocity displayed sharp peaks of velocity (Fig. 2 *b*). These short-lived speed bursts increased the overall variation of cell velocity, as measured by a high coefficient of variation (CV), which compares the standard deviation in velocity with its mean. Among the three different cases, only MDA-MB-231 cells in coculture conditions (case 3) demonstrated this pulsating migration and, accordingly, a high CV of instantaneous velocity (Fig. 3 *a*), i.e., fluctuations in the instantaneous speed of single MDA-MB-231 cells at low density or in a dense monolayer were small. These results suggest that nontransformed cells surrounding

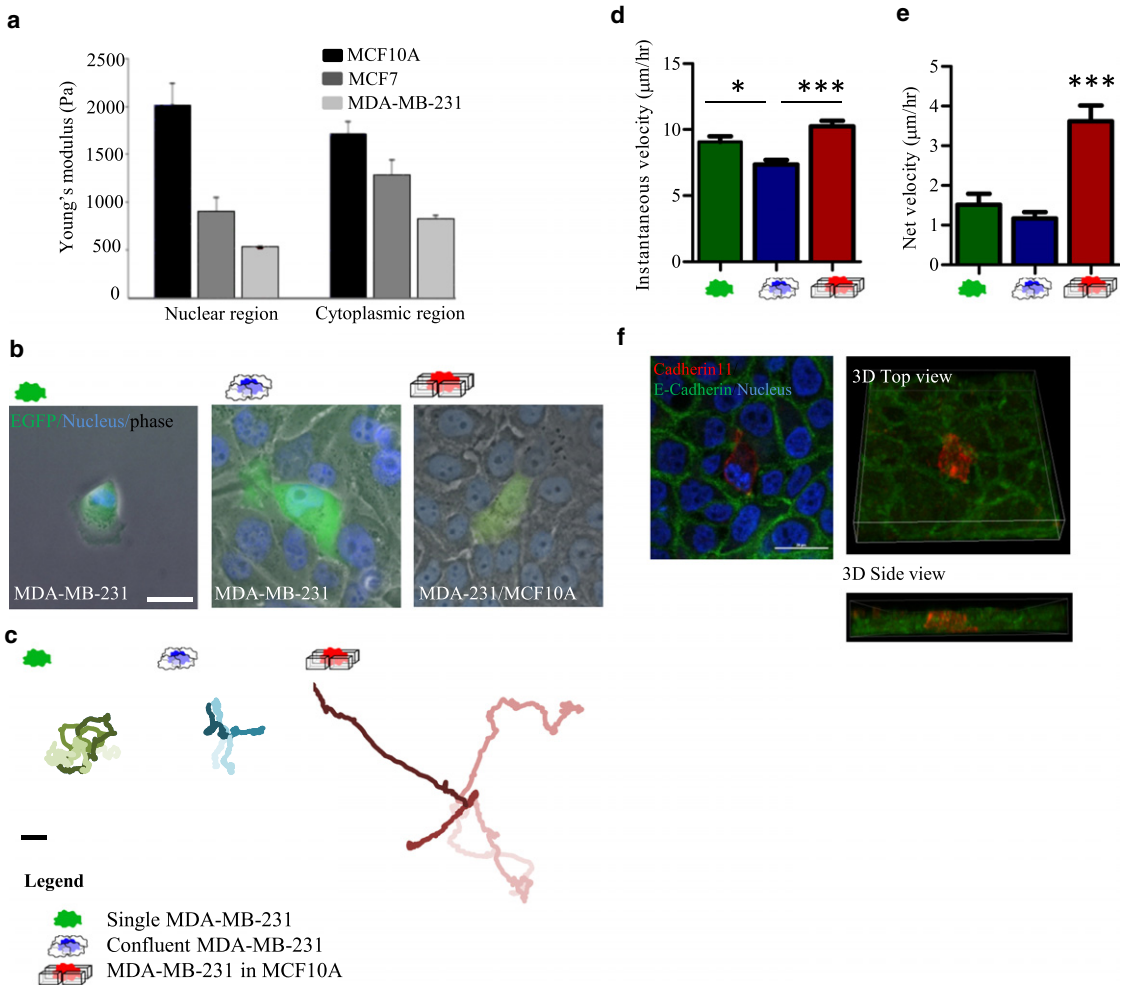

FIGURE 1 Motility of individual breast carcinoma cells (MDA-MB-231) is significantly enhanced when they are surrounded by normal breast epithelium cells (MCF10A). (*a*) Modal Young's moduli at indentation depths ranging from 200 to 300 nm of MDA-MB-231 and MCF10A cells. (*b*) For cell motility measurements, MDA-MB-231 cells were transduced with recombinant lentivirus encoding for EGFP and labeled with vital dye Hoechst 33342. The cells were cultured in the following three cases: 1), single MDA-MB-231 cells at low confluence; 2), a confluent monolayer of MDA-MB-231 cells; and 3), coculture in which single MDA-MB-231 cells were scattered in a confluent monolayer of nontransformed human breast epithelial cells (MCF10A). (*c–e*) The migratory behaviors of individual MDA-MB-231 were evaluated by means of 16-h-long movies. (*c*) Representative trajectories for the three different cases. (*d*) Instantaneous velocity and (*e*) net velocity of MDA-MB-231 cells for the three cases. (*f*) Immunofluorescence confocal image of the cells in coculture conditions in which MDA-MB-231and MCF10A cells were specifically labeled with cadherin 11 (*red*) or E-cadherin (*green*). Cell nuclei were stained with Hoechst 33342 (*blue*). 3D images were formed by reconstructing confocal *z*-stack images (magnification 60×; bar = 20 μm). Bar graphs show the mean ± SE of 11 independent experiments (***$p < 0.001$; **$p < 0.01$; *$p < 0.05$).

a single carcinoma cell in a monolayer can uniquely enhance its motility by inducing a pulsating or bursty mode of migration.

Enhanced cancer cell migration is induced by coordinated crowding of surrounding normal epithelial cells

What caused the pulsating migration of the MDA-MB-231 cells in a monolayer of nontransformed cells? As noted above, in coculture conditions, the sharply and transiently increased cell velocity of MDA-MB-231 cells was accompanied by the elongation of the cell body of the carcinoma cells, suggesting that these morphologic changes induced the observed pulsating migration of these cells. To test this hypothesis, we traced the time-dependent cell body and nucleus of carcinoma cells dispersed in a monolayer of nontransformed cells and computed their respective aspect ratios (i.e., the ratios of the lengths of the long and short axes). This analysis of the temporal profiles of cell and nuclear morphologies and cell speed indicated that the maximum peaks in the profiles of these three parameters overlapped (Fig. 2, *b–d*, *red curves*). Variations in nuclear (ARN) and cellular shape (ARC) were also much higher for carcinoma cells in monolayer than those for cases 1 and 2 (Fig. 3, *b* and *c*). Instead, the profiles of nuclear and cellular shape and instantaneous speed of the nontransformed cells in the monolayer were relatively flat (Fig. 2, *b* and *d*, *black curves*). The easy

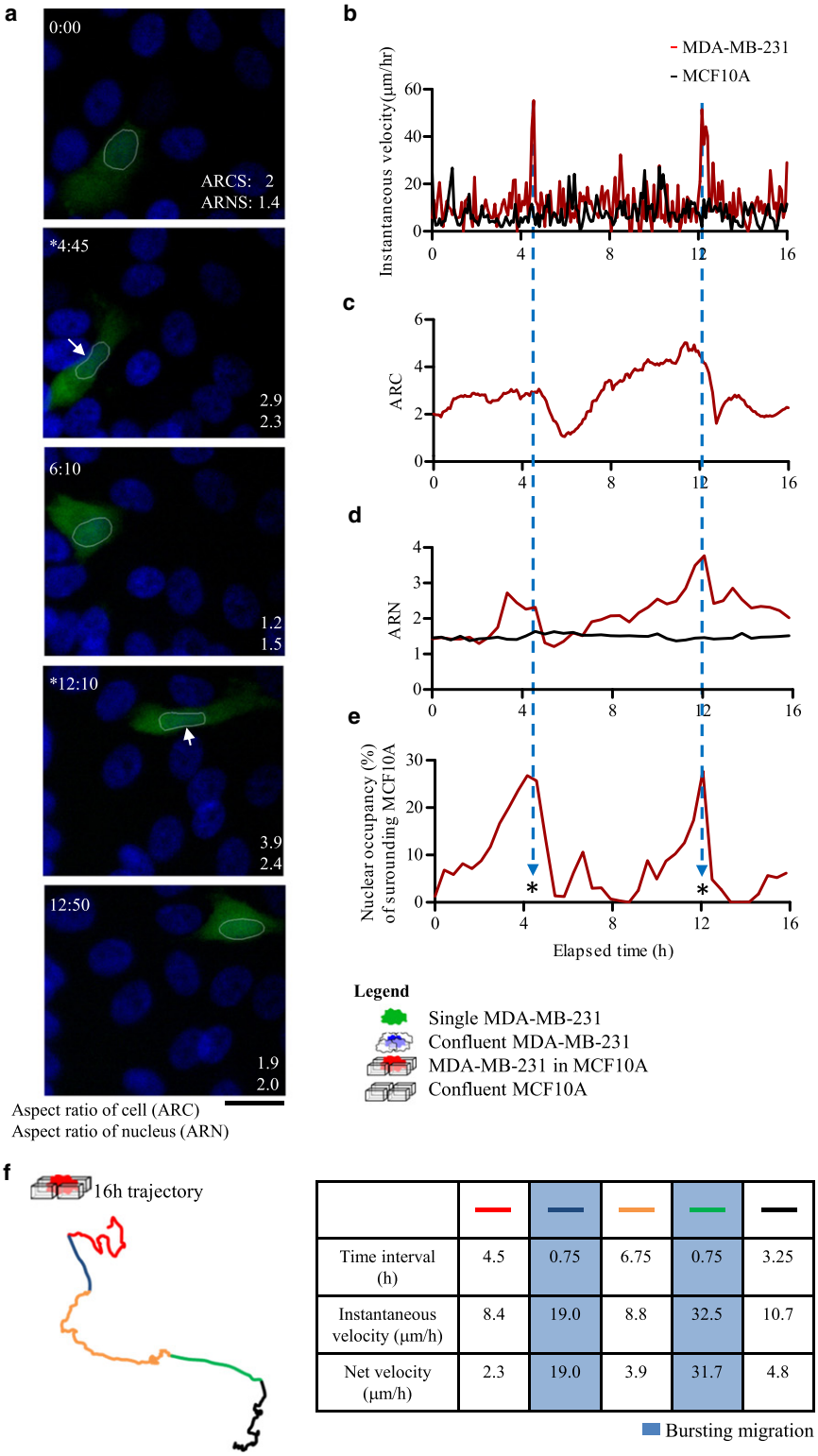

Time interval (h)	4.5	0.75	6.75	0.75	3.25
Instantaneous velocity (μm/h)	8.4	19.0	8.8	32.5	10.7
Net velocity (μm/h)	2.3	19.0	3.9	31.7	4.8

Bursting migration

FIGURE 2 Intermittent crowding of normal epithelial cells mediates the unique pulsating migration of MDA-MB-231 cells. (*a*) Time-dependent morphological changes in the cell body and nucleus of MDA-MB-231 in coculture conditions. The cell morphology and nuclear shape of individual MDA-MB-231 were visualized using EGFP (cytoplasm) and nuclear dye Hoechst 33342 (nuclear DNA). The aspect ratios of thcell (ARC) and nucleus (ARN) are indicated in the bottom right corner of each micrograph (magnification 40×; bar = 20 μm). (*b–e*) Temporal profiles of (*b*) instantaneous velocity, (*c*) ARC, (*d*) ARN, and (*e*) the nuclear occupancy of MCF10A cells around a MDA-MB-231 cell (i.e., the area of MCF10A cell nuclei in a 20 μm × 20 μm square around a MDA-MB-231 cell), obtained from one 16-h-long movie (five representative images are shown in panel *a*). The dashed lines represented the times at which bursts in cell speed of MDA-MB-231 occur. (*f*) The16-h-long trajectory of an MDA-MB-231 cells in a monolayer of MCF10A is segmented into color-coded excursions that represent short-lived episodes of fast, persistent migration interlaced with long episodes of slow, random migration.

stretching and convex deformation of the nucleus of MDA-MB-231 cells by MCF10A cells are consistent with the low modulus of the nucleus of MDA-MB-231 cells compared with the nuclear stiffness of MCF10A cells (Fig. 1 *a*). Whereas peaks in the velocity of the carcinoma cell were short-lived, the stretching of the cell and nucleus followed a slow buildup (Fig. 2, *c* and *d*) before going through their peaks (Fig. 2 *b*). This implies that the suddenly increased velocity of the carcinoma cell was preceded by a slow stretching of the cell body and nucleus.

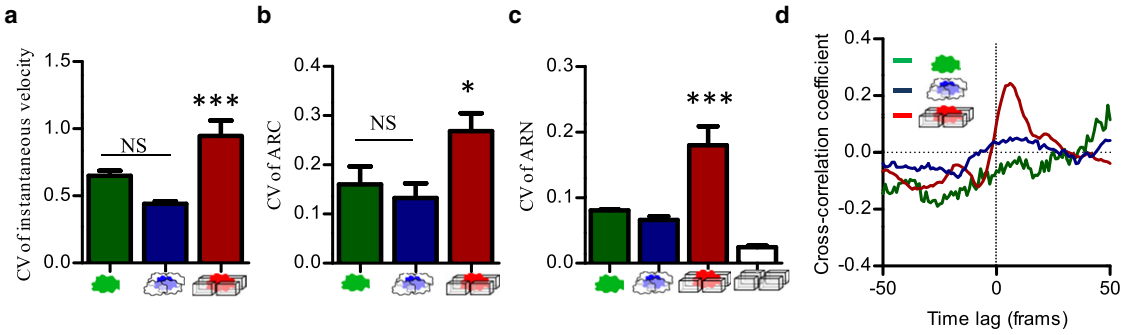

FIGURE 3 Speed bursts correlate with increases in overall variations in cell velocity, cell morphology, and nuclear shape. Cells were cultured in the following three cases: 1), single MDA-MB-231 cells at low confluence; 2), a confluent monolayer of MDA-MB-231 cells; and 3), coculture in which single MDA-MB-231 cells were scattered in a confluent monolayer of nontransformed human breast epithelial cells (MCF10A). (*a–c*) The bar graphs represent the mean ± SE of the CV of the (*a*) instantaneous velocity, (*b*) ARC, and (*c*) ARN for the three different cases within 16-h-long migration ($n = 11$; ***$p < 0.001$; **$p < 0.01$; *$p < 0.05$). (*d*) Average temporal cross-correlation between instantaneous velocity and ARCS of individual MDA-MB-231 cells in the three different cases ($n = 5$).

To establish pre-séance, we computed the temporal cross-correlation function between the instantaneous velocity of carcinoma cells and the aspect ratio of their cell body (Fig. 3 *d*). This analysis showed that the increased velocity was delayed relative to the high aspect ratio of cell shape, suggesting that the elongation of cell body preceded the observed bursts of velocity. The same analysis indicated that the correlation between cell speed and cell/nucleus shape did not exist in single (case 1) and confluent (case 2) MDA-MB-231 cells, both cases in which the pulsating motion was absent (Fig. 3 *c*).

To understand how nontransformed cells caused the dynamic morphological changes of cancer cells, we investigated the spatiotemporal distribution of MCF10A cells in close proximity to individual MDA-MB-231 cells in monolayer. First, we noted that in coculture, the nuclear shape of the nontransformed cells showed much less variation than that of carcinoma cells in the same monolayer (Fig. 2 *d*). As was previously shown for other types of cancer and nontransformed cells (14), this result suggests that the nucleus of the MCF10A cells was much stiffer than the nucleus of the MDA-MB-231 cells. Second, when they were transiently crowded by the nuclei of MCF10As (measured by a higher-than-average spatial density of these cells; *bottom panel* in Fig. 2 *a*), the MDA-MB-231 cells showed an elongated nucleus. During these crowding events, the curvature of the nucleus in MDA-MB-231 cells was often convex (Fig. 2 *a*, *arrows*). Inversely, when the nuclear density of MCF10A cells near the MDA-MB-231 cell was low (which was the majority of the time), the nucleus and cell body of the MDA-MB-231 cells were rounded (Fig. 2 *a*). The peaks in the profile of the nuclear occupancy of MCF10A cells around an MDA-MB-231 cell exactly matched the occurrence of sharply increased instantaneous velocity as well as the peaks in nuclear and cellular stretching (Fig. 2 *e*). Taken together, our results suggest that it is the intermittent crowding of individual MDA-MB-231 cells by the stiff nuclei of MCF10A cells that causes a cyclic stretch-shrink of the soft nucleus of the cancer cells (which is permissible thanks to the soft nucleus of the MDA-MB-231 cells), which in turn induces their singular pulsating migration.

Above, we identified biophysical factors that induced the enhanced motility of cancer cells in a monolayer of nontransformed cells. Below, we determine critical molecular mechanisms that underlie this phenomenon. To further assess the impact of MCF10A cells on the motility of MDA-MB-231 cells, we examined whether independently reducing the motion of nontransformed cells inhibited the pulsating migration of cancer cells. To that end, we first investigated the mechanism of movements of MCF10A cells in confluent monolayers (with no MDA-MB-231 cells present). Confluent MCF10A cells formed actin filament bundles parallel to E-cadherin-rich adherens junctions at cell-cell contact sites (Fig. S4 *a*). It is commonly accepted that actin bundle structures stabilize adherens junctions and maintain cell-cell contacts (15,16). However, whether the formation of an actin bundle limits the net migration of connecting cells in monolayer is unclear. To examine this issue, we expressed the actin probe EGFP-lifeact (17,18) to visualize the dynamic actin organization in live cells. We found that actin filament bundles were formed and localized at the cortical interface of connecting cells, but the width of this actin cortex changed dynamically as one cell moved away and then formed a new connection with other cells (Fig. 4 *a*), indicating the migratory ability of individual MCF10A cells in confluent conditions. To further understand the function of bundled actin, we treated MCF10A cells with latrunculin B, an inhibitor of actin polymerization. Treatment with as little as 80 nM latrunculin B disrupted the organization of the actin filament bundles, as evidenced by the wider appearance of the phalloidin stain (Fig. S4 *b*). Importantly, the net velocity dropped by 40% after treatment with latrunculin B (Fig. 4, *b–e*), suggesting

that actin bundles drive the motion of individual nontransformed cells in confluent conditions.

Role of α-catenin in bursty cancer cell migration

Because recent studies have shown the critical role of α-catenin in promoting actin filament bundle formation (16,19) as well as intercellular adhesion (20,21), we examined whether depleting α-catenin inhibited the motion of individual MCF10A cell in coculture conditions. First, α-catenin was depleted in MCF10As with the use of shRNA encoding recombinant lentivirus (MCF10A si-α-cat; Fig. S5). The MCF10A si-α-cat cells formed branched actin projecting from the edge of the cells and failed to form actin bundles (Fig. 4 *f*). Accordingly, the MCF10A si-α-cat cells showed both reduced instantaneous speed and reduced net speed (Fig. 4, *g–i*), which suggests that the inability of these cells to form tight actin filament bundles and form mature adherens junctions limits the motion of individual MCF10As in confluent conditions.

Next, we examined the migratory behavior of single MDA-MB-231 cells in a confluent monolayer of MCF10A si-α-cat cells. We previously demonstrated that the depletion of α-catenin reduces cell-cell adhesion by reducing E-cadherin/E-cadherin affinity (21). If cancer cells merely squeeze between nontransformed cells (a steric-based model of migration), then reduced adhesion between normal cells induced by α-catenin depletion should increase the cancer cell speed. If, instead, according to our proposed mechanism, the cancer cell speed is enhanced by nuclear crowding, then reduced adhesion between normal cells should decrease the cancer cell speed. We found that MCF10A si-α-cat cells had a smaller impact on MDA-MB-231 cells, as evidenced by a significantly reduced variation in cell morphology and nucleus shape (Fig. 4, *k* and *l*). Accordingly, the indicating parameters of the pulsating migration of MDA-MB-231 cells, including a high CV of instantaneous velocity and high temporal correlation between cell shape and instantaneous velocity, were absent (Fig. 4 *j*). MDA-MB-231 cells were effectively immobilized in confluent monolayers of MCF10A si-α-cat cells (Movie S4), resulting in dramatically reduced instantaneous and net velocity of MDA-MB-231 cells compared with their speed in monolayers of control MCF10A cells (Fig. 4, *m* and *n*). Thus, we conclude that the pulsating migration of a cancer cell in a monolayer of nontransformed cells critically depends on the coordinated motion of nontransformed cells mediated by α-catenin-based adhesive forces generated by actin filament bundles at adherens junctions.

Because a recent study indicated that the secreted factors from nontransformed epithelial cells increase the motility of breast cancer cells (22), we next sought to determine whether the chemical stimuli generated by nontransformed cells were at least partially responsible for the enhanced migratory behavior of the carcinoma cells. The conditioned medium of both MCF10A and MCF10A si-α-cat stimulated MDA-MB-231 motility (evident as long, straight trajectories with slightly increased net velocity), whereas the conditioned medium of MDA-MB-231 did not induce enhanced migration, implying the specific influence of factors secreted by MCF10A cells (Fig. S6, *a–c*). However, important characteristics of the observed pulsating migration, including the high CV of instantaneous velocity and the high temporal correlation between cell shape and instantaneous velocity, were absent in the treatment of MDA-MB-231 by MCF10A si-α-cat conditioned medium (Fig. S6, *d–f*), indicating that secreted proteins and direct contact forces by nontransformed cells enhance cancer migration through different mechanisms. Specifically, we have shown that direct coculture with MCF10A si-α-cat cells blocked the migration of MDA-MB-231 cells, as opposed to the treatment of only MCF10A si-α-cat conditioned medium, suggesting that physical contact is the dominant factor that determines the enhanced net migration of carcinoma cells in a monolayer.

Bursty migration of invasive versus noninvasive cancer cells

Next, we sought to determine whether MCF10A cells induce different extents of pulsating motion in invasive and noninvasive cancer cells. To that end, we compared the migratory behavior of single, noninvasive breast cancer MCF7 cells with that of single, invasive MDA-MB-231 cells, both in coculture conditions with MCF10A cells (Fig. 5 *a* and Movie S5). The MCF7 cells showed significantly lower instantaneous velocity (Fig. 5 *d*) and net velocity (Fig. 5 *e*), and less variation in cell morphology, nucleus shape, and cell speed than the MDA-MB-231 cells (Fig. 5, *f–h*), indicating that pulsating migration was absent in these cells. Although the CV of instantaneous velocity was not reduced, the significant decrease in instantaneous velocity still indicated the lack of enhanced migration in MCF7 cells. Overall, the MCF7 cells did not undergo pulsating migration within a confluent monolayer of MCF10A cells, and were effectively stuck in the monolayer of nontransformed cells (Fig. S7). These results suggest that invasive cancer cells are more susceptible to normal-cell-induced pulsating migration, and enhanced migration may be due to the loss of E-cadherin.

The above observation raises the question: How can invasive (but not noninvasive) cancer cells overcome the steric and adhesive forces of surrounding normal cells, and even exploit them to undergo large net displacements? Because loss of E-cadherin commonly occurs in metastatic cancer cells (23,24), and MCF7 cells (but not MDA-MB-231 cells) express E-cadherin (25), we investigated whether E-cadherin-mediated adherens junctions could erase the impact of normal cells on cancer cell motility. We employed a gain-of-function approach by supplying E-cadherin

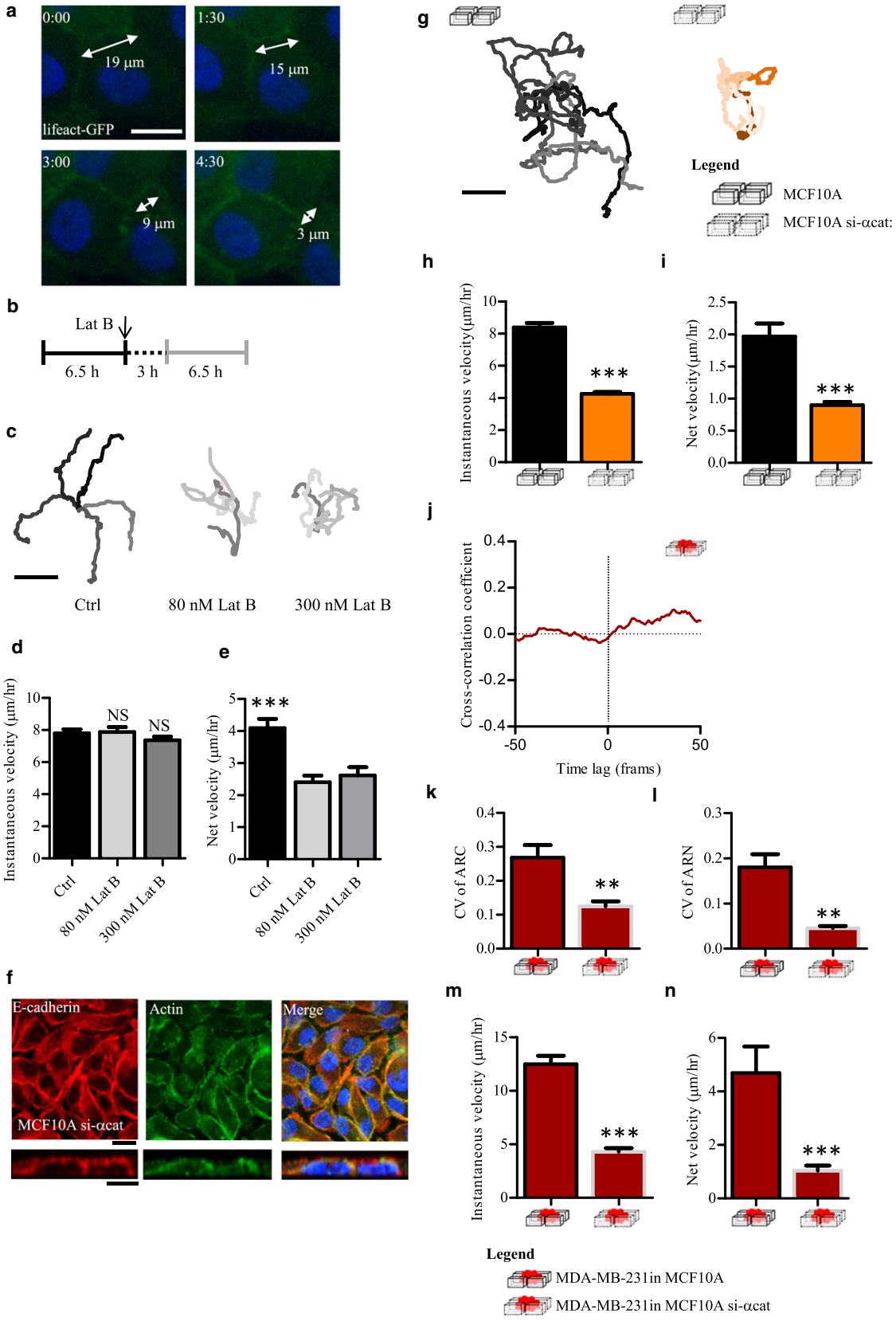

FIGURE 4 Pulsating migration of single cancer cells depends on the coordinated motion of normal cells. (*a*) Time-dependent actin organization in confluent MCF10 cells in which the actin probe lifeact-EGFP was expressed with the use of a lentiviral gene transfer system. The width of actin filament bundles localized at the cortical interface of connecting cells was measured in each image. (*b–e*) The migratory speed of MCF10A cells in a confluent

exogenously to MDA-MB-231 cells, which do not normally express E-cadherin. E-cadherin-EGFP fusion protein distributed to the cytoplasm and the cell periphery (Fig. 5 *b*). Unlike control cells, MDA-MB-231 cells expressing E-cadherin formed overt cell-cell contacts, suggesting that exogenous E-cadherin mediated the formation of adherens junctions. Importantly, the forced expression of E-cadherin in MDA-MB-231 cells diminished their pulsating migratory response to MCF10A cells, to the same extent as for MCF7 cells (Fig. 5, *d–h*). The instantaneous and net velocities both decreased because speed bursts largely vanished (Fig. 5, *d–h*, and Fig. S7). We conclude that E-cadherin-based cell-cell adhesions determine the amplitude of the pulsating migration of cancer cells induced by MCF10A cells.

DISCUSSION

Our results support the hypothesis that differences in the mechanical stiffness of the cytoplasm and nucleus, as well as intercellular adhesive properties (two well-established features of cancer cells in comparison with normal cells) can induce a novel mechanism of migration in a cell monolayer. The high net migration of an individual soft cancer cell is caused by its transient caging by the stiff surrounding normal cells, which build up mechanical stress that deforms the nucleus and cytoplasm of the cancer cell, until this deformation becomes unstable and the soft cell makes it to the next cage in the monolayer. This transient caging phenomenon exhibited by nontransformed cells is itself mediated by their tight α-catenin/E-cadherin-based intercellular adhesion, i.e., surprisingly, only tight connections among surrounding stiff cells can coordinately push the soft cell. Pulsating/bursty migration does not occur in E-cadherin-expressing, noninvasive cancer cells, and is eliminated by exogenously expressing E-cadherin in invasive cancer cells. Although force transduction among cells could involve mechanisms that are not based on the cadherin/α-catenin complex, we note that the bursty migration was almost completely abrogated when the MDA-MB-231 cells were in contact with α-catenin-depleted MCF10A cells, which suggests that cadherin/catenin-mediated force transduction is dominant.

This pulsating motion is characterized by cycles of large morphological changes corresponding to repeated phases of cell extension and contraction. These repeated cycles are induced by surrounding stiff epithelial cells, not by interactions of the cancer cell with the substratum as in the cases of conventional mesenchymal migration and amoeboid migration (26,27). Physical forces locally applied to the cell surface have been demonstrated to induce local activation of small GTPases, the known mediators of actin assembly and actomyosin contractility (28). Here, we found that such forces are applied on the lateral surfaces of the individual cancer cells by the surrounding epithelial cells. In addition, we showed that invasive cancer cells (MDA-MB-231) were significantly softer than noninvasive cancer cells (MCF7), which makes invasive cancer cells more sensitive to physical forces (29). Together, these results suggest that the continuous impinging forces induced by epithelia cells, particularly through their stiff nucleus, cause actin assembly and actomyosin contractility through GTPase activation, which facilitates the active deformation of the soft invasive cancer cells, and in turn enables them to undergo pulsating migration. We note that episodes of net cell migration are of short duration compared with cellular deformations because cell migration is driven by a mechanical instability. A nuclear deformation that is convex (dog-bone shaped; Fig. 2 *a*) is highly unstable and can only be relaxed by net cell movement to release this energetically unfavorable deformation and turn the nucleus back into an energetically favorable rounded shape.

Within the 16-h observation window, the shape of the cell body and the nucleus remained constant in the stiff cells of the confluent monolayer. An interesting question then arises: How does each stiff cell of the monolayer balance the forces generated by its surrounding stiff cells, which cause morphologic changes of the soft cells? This possible protective mechanism stems partly from the stiffness of epithelial cells and partly from E-cadherin-mediated adherens junctions at cell-cell contact sites. After two cells form hemophilic E-cadherin binding, activated myosin II generates tugging forces to prevent further impingement (30,31). Hence, epithelial cells do not experience the full contact forces generated by neighboring cells, in contrast to the cancer cells lacking E-cadherin. Indeed, after we introduced E-cadherin into MDA-MB-231, which enabled them to form adherens junctions, these cells resisted the contact forces from surrounding MCF10A cells, as suggested by the significantly reduced morphological deformations of the E-cadherin-expressing MDA-MB-231 cells. In turn, these cells lost their ability to undergo pulsating migration and were stably trapped in epithelial cages. Taken

monolayer in the absence of latrunculin B (Lat B, 80 or 300 nM) was first monitored for 6.5 h (ctrl). After 3 h, the movements of Lat B-treated cells were monitored for another 6.5 h. (*c*) Five representative trajectories. (*d* and *e*) Instantaneous velocity (*d*) and net velocity (*e*) of ctrl, 80 nM Lat B, and 300 nM LatB-treated cells. (*f–i*) MCF10A cells were transduced with recombinant lentivirus encoding for shRNA targeting the α-catenin mRNA (MCF10A si-α-cat). (*f*) Confocal images of confluent MCF10A si-α-cat cells stained with actin phalloidin (*red*) and E-cadherin (*green*). The nuclei were visualized with Hoechst 33342 (*blue*). The bottom panel shows the lateral cross sections obtained by maximum intensity projection from confocal *z*-stack images. Scale bar = 20 μm. (*g*) Five representative trajectories. (*h* and *i*) Instantaneous velocity (*h*) and net velocity (*i*) of MCF10A si-α-cat compared with MCF10A from 16-h-long movies. (*j–n*) Single MDA-MB-231 cells were scattered in a confluent monolayer of MCF10A si-α-cat. (*j*) The average temporal cross-correlation between instantaneous velocity and ARC of MDA-MB-231 ($n = 5$). (*k–n*) The CVs of (*k*) ARC, (*l*) ARN, (*m*) instantaneous velocity, and (*n*) net velocity from 16-h-long movies are shown in bar graphs (mean $\pm$ SE; $n = 11$; $^{***}p < 0.001$; $^{**}p < 0.01$; $^{*}p < 0.05$).

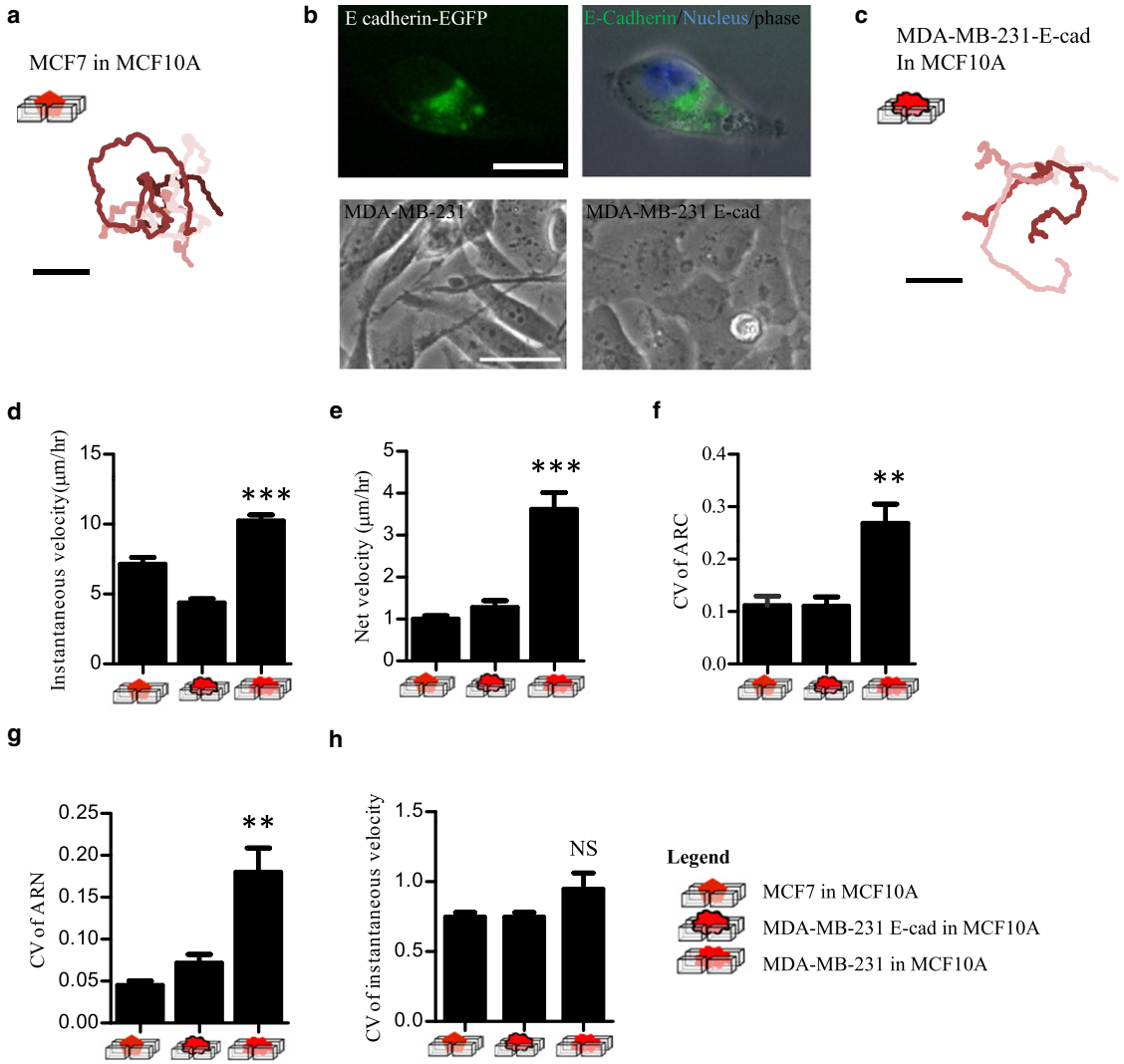

FIGURE 5 E-cadherin-based cell-cell adhesions determine the amplitude of the pulsating migration of cancer cells induced by normal cells. (*a*) Five representative 16-h-long migratory trajectories of noninvasive breast cancer MCF7 cells (which express E-cadherin) scattered in a confluent monolayer of MCF10A cells (which also express E-cadherin). (*b* and *c*) MDA-MB-231 cells (which lack E-cadherin) were transduced with full-length E-cadherin fused with EGFP (MDA-MB-231 E-cad). (*b*) Upper panels: Fluorescent micrograph of exogenously expressed E-cadherin in single MDA-MB-231 E-cadherin cells (*right*: E-cadherin-EGFP; *left*: merged image of E-cadherin-EGFP (*green*), Hoechst 33342 (*blue*), and phase contrast). Lower panels: Phase images of confluent MDA-MB-231 and MDA-MB-231 E-cadherin. (*c*) Five representative 16-h-long migratory trajectories of MDA-MB-231 cells expressing E-cadherin scattered in a confluent monolayer of MCF10A cells. (*d–h*) The bar graphs represent the mean ± SE of the (*d*) instantaneous velocity, (*e*) net velocity, (*f*) CV of ARC, (*g*) CV of ARN, and (*h*) CV of instantaneous velocity of MCF7 cells, E-cadherin-expressing MDA-MB-231 cells, and MDA-MB-231 cells in a monolayer with MCF10A cells from 16-h-long movies ($n = 11$; $^{***}p < 0.001$; $^{**}p < 0.01$; $^{*}p < 0.05$). Scale bar = 20 μm.

together, these experiments demonstrate that the loss of E-cadherin is not only a marker of epithelial–mesenchymal transition but also switches carcinoma cells from a mode of migration in which net velocity is low because of steric constraints caused by surrounding cells to a fast pulsating mode of migration, which is coordinately mediated by surrounding cells of the monolayer.

Accumulating evidence indicates that dissemination and metastasis constitute an early event in tumor progression and may occur before tumor growth (32,33). Epithelial–mesenchymal transition is believed to be a consequence of the loss of expression in E-cadherin. Here, we have shown that as soon as a few cells lose E-cadherin, the surrounding nontransformed E-cadherin-expressing cells of the epithelium can participate in pushing these transformed cells to undergo a rapid net migration. Hence, our experiments reveal the nonnegligible role of surrounding stiff cells in promoting the rapid metastatic spread of individual cancer cells before tumor growth occurs. Therefore, inhibiting or reducing the movement of normal epithelial cells may provide a new therapeutic strategy to block early metastasis. In a confluent epithelial tissue, the formation of adherens junctions generates two opposite forces—adhesive forces and cortical tension—that respectively enable individual

cells to extend or contract their contact area with neighbors (30). By gradually remodeling their adhesion with new neighbors, individual epithelial cells can move from one cage to the next. This mechanism suggests that it is possible to control the motion of individual cells in an epithelial monolayer by impairing the adherens junctions. Indeed, our experiments demonstrate that the depletion of α-catenin, a molecule that stabilizes cell-cell adhesion (13), serves to brake the motion of MCF10A cells, such that the soft cancer cells are effectively immobilized. Overall, these results shed light on the role of surrounding stiff epithelial cells in early steps of cancer dissemination.

SUPPORTING MATERIAL

Seven figures and five movies are available at http://www.biophysj.org/biophysj/supplemental/S0006-3495(12)00557-7.

This work was supported by National Institutes of Health grants R01GM084204, U54CA143868, and U54CA143862.

REFERENCES

1. Ma, L., S. Yamada, …, P. A. Coulombe. 2001. A 'hot-spot' mutation alters the mechanical properties of keratin filament networks. *Nat. Cell Biol.* 3:503–506.
2. Sivaramakrishnan, S., J. V. DeGiulio, …, K. M. Ridge. 2008. Micromechanical properties of keratin intermediate filament networks. *Proc. Natl. Acad. Sci. USA.* 105:889–894.
3. Lammerding, J., P. C. Schulze, …, R. T. Lee. 2004. Lamin A/C deficiency causes defective nuclear mechanics and mechanotransduction. *J. Clin. Invest.* 113:370–378.
4. Stewart-Hutchinson, P. J., C. M. Hale, …, D. Hodzic. 2008. Structural requirements for the assembly of LINC complexes and their function in cellular mechanical stiffness. *Exp. Cell Res.* 314:1892–1905.
5. Wirtz, D., K. Konstantopoulos, and P. C. Searson. 2011. The physics of cancer: the role of physical interactions and mechanical forces in metastasis. *Nat. Rev. Cancer.* 11:512–522.
6. Cross, S. E., Y. S. Jin, …, J. K. Gimzewski. 2007. Nanomechanical analysis of cells from cancer patients. *Nat. Nanotechnol.* 2:780–783.
7. Guck, J., S. Schinkinger, …, C. Bilby. 2005. Optical deformability as an inherent cell marker for testing malignant transformation and metastatic competence. *Biophys. J.* 88:3689–3698.
8. Walter, N., T. Busch, …, J. P. Spatz. 2011. Elastic moduli of living epithelial pancreatic cancer cells and their skeletonized keratin intermediate filament network. *Biointerphases.* 6:79–85.
9. Suresh, S. 2007. Nanomedicine: elastic clues in cancer detection. *Nat. Nanotechnol.* 2:748–749.
10. Swaminathan, V., K. Mythreye, …, R. Superfine. 2011. Mechanical stiffness grades metastatic potential in patient tumor cells and in cancer cell lines. *Cancer Res.* 71:5075–5080.
11. Lee, M. H., R. Padmashali, and S. T. Andreadis. 2011. JNK1 is required for lentivirus entry and gene transfer. *J. Virol.* 85:2657–2665.
12. Altenburger, R., M. Schmitt-Jansen, and J. Riedl. 2008. Bioassays with unicellular algae: deviations from exponential growth and its implications for toxicity test results. *J. Environ. Qual.* 37:16–21.
13. Panorchan, P., M. S. Thompson, …, D. Wirtz. 2006. Single-molecule analysis of cadherin-mediated cell-cell adhesion. *J. Cell Sci.* 119: 66–74.
14. Zink, D., A. H. Fischer, and J. A. Nickerson. 2004. Nuclear structure in cancer cells. *Nat. Rev. Cancer.* 4:677–687.
15. Vasioukhin, V., C. Bauer, …, E. Fuchs. 2000. Directed actin polymerization is the driving force for epithelial cell-cell adhesion. *Cell.* 100:209–219.
16. Lee, M. H., R. Padmashali, P. Koria, and S. T. Andreadis. 2011. JNK regulates binding of α-catenin to adherens junctions and cell-cell adhesion. *FASEB J.* 25:613–623.
17. Riedl, J., A. H. Crevenna, …, R. Wedlich-Soldner. 2008. Lifeact: a versatile marker to visualize F-actin. *Nat. Methods.* 5:605–607.
18. Khatau, S. B., C. M. Hale, …, D. Wirtz. 2009. A perinuclear actin cap regulates nuclear shape. *Proc. Natl. Acad. Sci. USA.* 106:19017–19022.
19. Drees, F., S. Pokutta, …, W. I. Weis. 2005. α-Catenin is a molecular switch that binds E-cadherin-β-catenin and regulates actin-filament assembly. *Cell.* 123:903–915.
20. Bajpai, S., J. Correia, …, D. Wirtz. 2008. α-Catenin mediates initial E-cadherin-dependent cell-cell recognition and subsequent bond strengthening. *Proc. Natl. Acad. Sci. USA.* 105:18331–18336.
21. Bajpai, S., Y. Feng, …, D. Wirtz. 2009. Loss of α-catenin decreases the strength of single E-cadherin bonds between human cancer cells. *J. Biol. Chem.* 284:18252–18259.
22. Carpenter, P. M., A. V. Dao, …, S. P. Wilczynski. 2009. Motility induction in breast carcinoma by mammary epithelial laminin 332 (laminin 5). *Mol. Cancer Res.* 7:462–475.
23. Hanahan, D., and R. A. Weinberg. 2011. Hallmarks of cancer: the next generation. *Cell.* 144:646–674.
24. Thiery, J. P., and J. P. Sleeman. 2006. Complex networks orchestrate epithelial-mesenchymal transitions. *Nat. Rev. Mol. Cell Biol.* 7: 131–142.
25. Nieman, M. T., R. S. Prudoff, …, M. J. Wheelock. 1999. N-cadherin promotes motility in human breast cancer cells regardless of their E-cadherin expression. *J. Cell Biol.* 147:631–644.
26. Binamé, F., G. Pawlak, …, U. Hibner. 2010. What makes cells move: requirements and obstacles for spontaneous cell motility. *Mol. Biosyst.* 6:648–661.
27. Friedl, P. 2004. Prespecification and plasticity: shifting mechanisms of cell migration. *Curr. Opin. Cell Biol.* 16:14–23.
28. Poh, Y. C., S. Na, …, N. Wang. 2009. Rapid activation of Rac GTPase in living cells by force is independent of Src. *PLoS ONE.* 4:e7886.
29. Irimia, D., and M. Toner. 2009. Spontaneous migration of cancer cells under conditions of mechanical confinement. *Integr. Biol.* 1:506–512.
30. Cavey, M., and T. Lecuit. 2009. Molecular bases of cell-cell junctions stability and dynamics. *Cold Spring Harb. Perspect. Biol.* 1:a002998.
31. Liu, Z., J. L. Tan, …, C. S. Chen. 2010. Mechanical tugging force regulates the size of cell-cell junctions. *Proc. Natl. Acad. Sci. USA.* 107:9944–9949.
32. Hüsemann, Y., J. B. Geigl, …, C. A. Klein. 2008. Systemic spread is an early step in breast cancer. *Cancer Cell.* 13:58–68.
33. Schmidt-Kittler, O., T. Ragg, …, C. A. Klein. 2003. From latent disseminated cells to overt metastasis: genetic analysis of systemic breast cancer progression. *Proc. Natl. Acad. Sci. USA.* 100:7737–7742.

Supplemental Figures

Mismatch in mechanical and adhesive properties induces pulsating cancer cell migration in epithelial monolayer

Meng-Horng Lee, Pei-Hsun Wu, Jack Rory Staunton, Robert Ros, Gregory D. Longmore, and Denis Wirtz

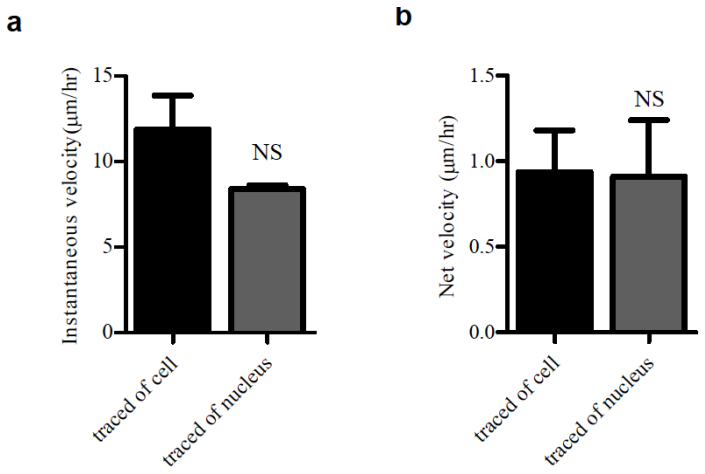

Fig. S1

Figure S1: Similar migratory speeds were obtained by tracing the time-dependent trajectories of cells and tracing their nuclei. MDA-MB-231 cells were transduced with recombinant lentivirus encoding for EGFP and labeled with vital dye Hoechst33342. 16-h-long movies were collected and the migratory speeds of individual MDA-MB-231 were evaluated by either tracing the centroid of cell body indicated by EGFP signal or the centroid of the nucleus indicated by Hoechst33342. The bar graphs represent the mean ± SEM of **(a)** instantaneous velocity and **(b)** net velocity. (n=3, NS: $P > 0.05$).

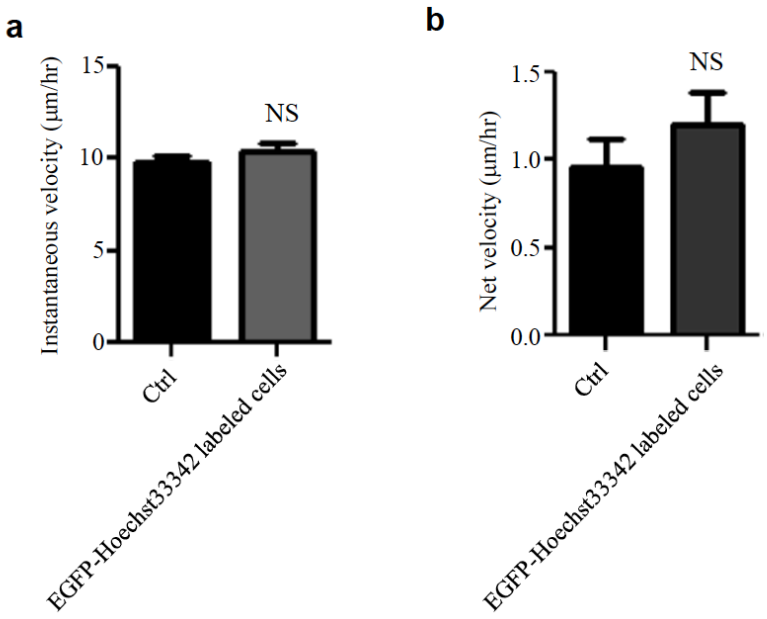

Fig. S2

Figure S2: The motility of individual breast carcinoma cells is unaffected by EGFP expression and Hoechst33342 labeling. MDA-MB-231 cells were either untreated or transduced with recombinant lentivirus encoding for EGFP and labeled with vital dye Hoechst33342. The migratory speed of individual MDA-MB-231 was evaluated by collecting 16-h-long movies. The bar graphs represent the mean ± SEM of **(a)** instantaneous velocity and **(d)** net velocity. (n=7, NS: $P > 0.05$).

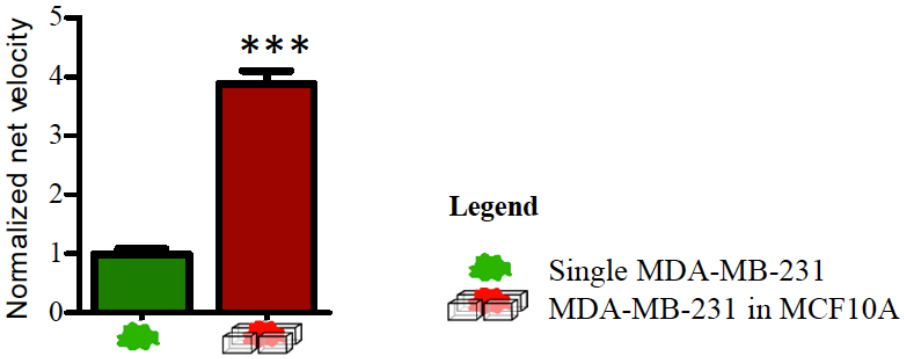

Fig. S3

Figure S3: The net velocity of individual breast carcinoma cells (MDA-MB-231) is significantly enhanced when surrounded by normal breast epithelium cells (MCF10A). The net velocity of individual MDA-MB-231 in single cell (case I) and co-culture (case III) conditions were compared by collecting 16-h-long movies (magnification 10X). The bar graphs represent the mean ± SEM of net velocity. (n=150, ***: $P < 0.001$).

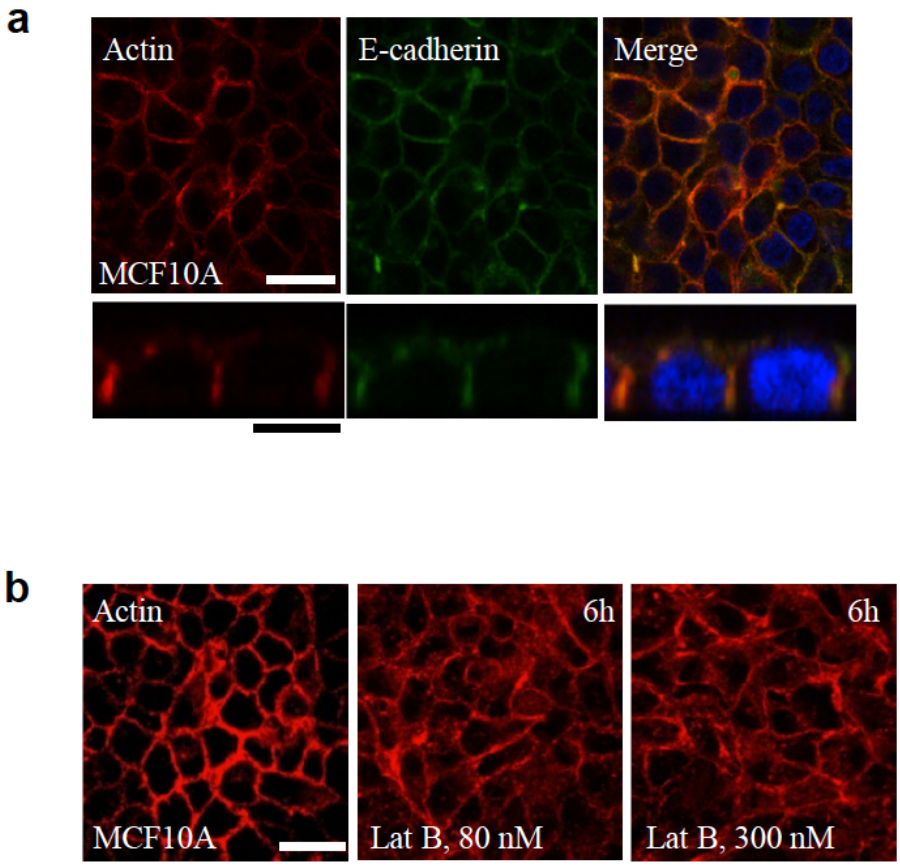

Fig. S4

Figure S4: Actin filament and E-cadherin organization in MCF10A cell monolayer. **(a)** Immunofluorescence confocal images of MCF10A cells stained with actin phalloidin (red) and E-cadherin (green). Nuclei were visualized with Hoechst 33342 (blue). Bottom panel shows the lateral crossections obtained by maximum intensity projections from confocal z-stack images. **(b)** Confluent MCF10A cells were treated with either vehicle or latrunculin B (80 nM or 300 nM) for 6h. Confocal images of the cells stained with actin phalloidin (green). Scale bar, 20 μm.

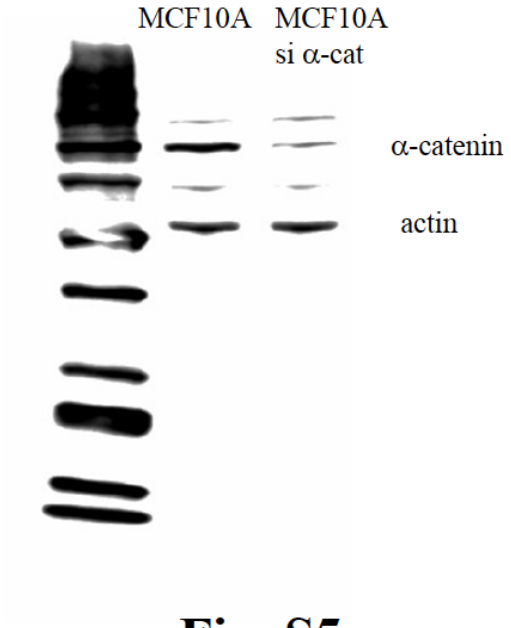

Fig. S5

Figure S5: α-catenin was depleted in MCF10As. MCF10A cells were transduced with recombinant lentivirus encoding for shRNA targeting the *α-catenin* mRNA (si-α-cat). The amount α-catenin in MCF10A and MCF10A si α-cat were detected using Western blotting. Actin was used as loading control

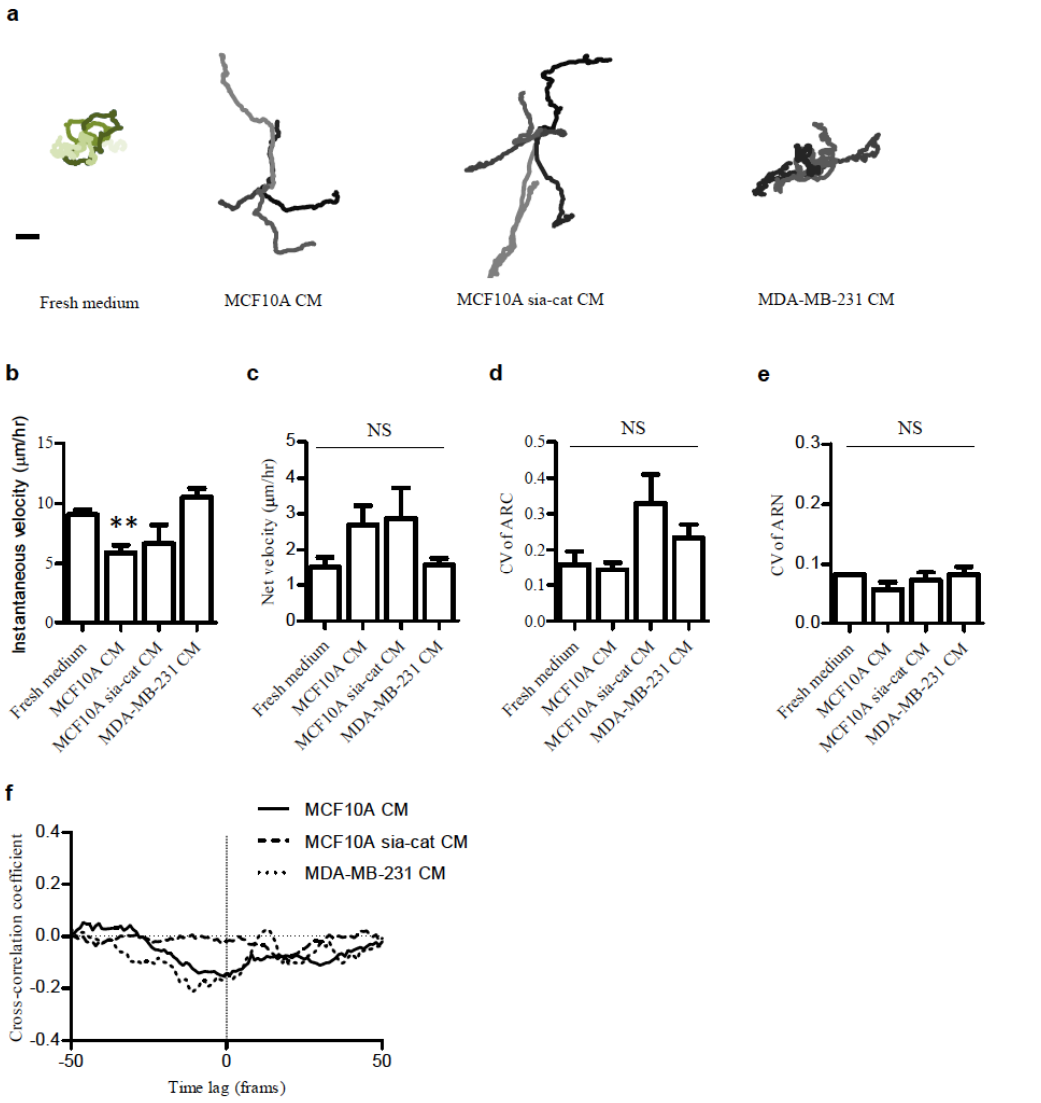

Fig. S6

Figure S6. Effect of conditioned medium on single-cell migration. (**a**) Typical trajectories of individual MDA-MB-231 cells in fresh MCF10A cell culture medium, in MCF10A conditioned medium, in culture medium from MCF10A cells depleted of α-catenin (MCF10A si α-cat), and in MDA-MB-231 conditioned medium. **(b-e)** The bar graphs represent the mean ± SEM of **(b)** the instantaneous velocity **(c)** the net velocity, the coefficient of variation (CV) of **(d)** the ARC and **(e)** the ARN for the three different cases. (n=11; NS=non-significant; **: P< 0.01) **(i)** Average temporal cross-correlation between instantaneous velocity and ARC of individual MDA-MB-231 cells in the three different cases (n=5).

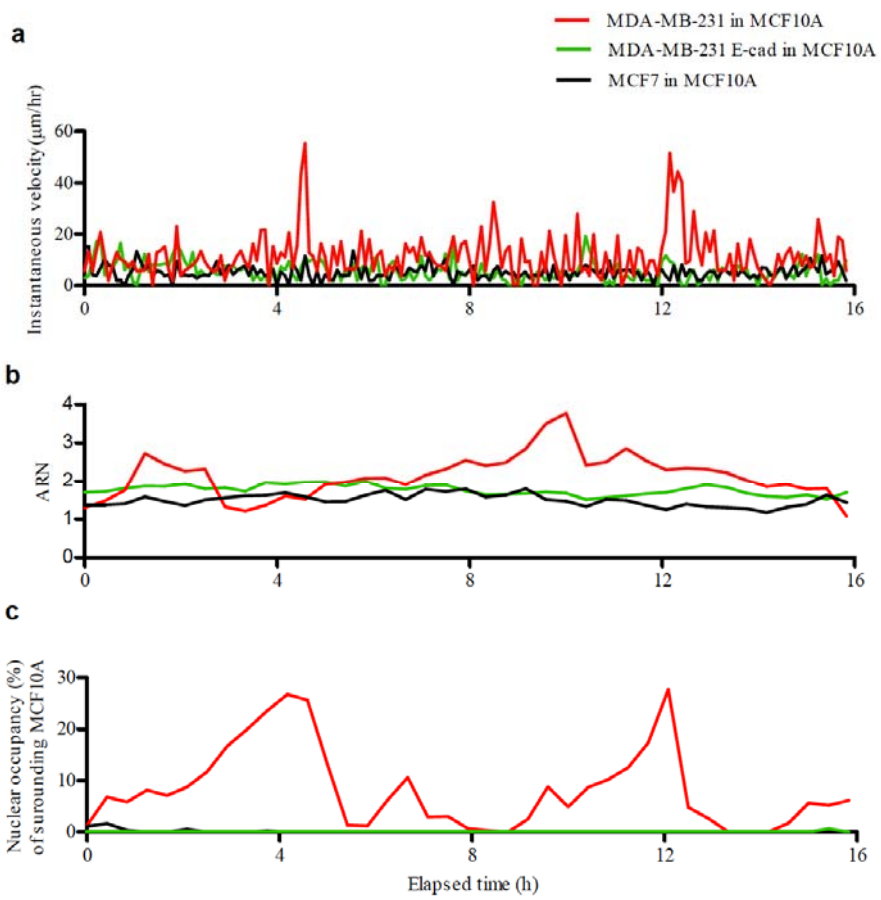

Fig. S7

Figure S7: Loss of E-cadherin in cancer cells is required for their pulsating migration induced by normal cells. MDA-MB-231 (red line), MDA-MB-231 E-cad (which express E-cadherin, green line), or MCF7 cells (black line) were scattered in a confluent monolayer of MCF10A cells and their migratory behaviors were evaluated by collecting 16-h-long movies. **(a-c)** Temporal profiles of **(a)** instantaneous velocity, **(b)** aspect ratio of nucleus (ARN), and **(c)** the nuclear occupancy of MCF10A cells around a MDA-MB-231 or MCF7 cell (i.e. the area of MCF10A cell nuclei in a 20 μm by 20 μm square around a MDA-MB-231 cell).

Supplemental videos

Video 1: The 16-h-long movies of individual MDA-MB-231 (case I). Scale bar=20 μm

Video 2: The 16-h-long movies of confluent monolayer of MDA-MB-231 cells (case II). Scale bar=20 μm

Video 3: The 16-h-long movies of individual MDA-MB-231 scattered in a confluent monolayer of MCF10A. Scale bar=20 μm

Video 4: The 16-h-long movies of individual MDA-MB-231 scattered in a confluent monolayer of MCF10A si α-cat cells. Scale bar=20 μm

Video 5: The 16-h-long movies of individual MCF7 scattered in a confluent monolayer of MCF10A. Scale bar=20 μm